Journal of Magnetism and Magnetic Materials 419 (2016) 156–165

Contents lists available at ScienceDirect

Journal of Magnetism and Magnetic Materials

journal homepage: www.elsevier.com/locate/jmmm

Effects of strain-induced martensite and its reversion on the magnetic properties of AISI 201 austenitic stainless steel

I.R. Souza Filho [a], M.J.R. Sandim [a,*], R. Cohen [b], L.C.C.M. Nagamine [b], J. Hoffmann [c], R.E. Bolmaro [d], H.R.Z. Sandim [a]

[a] Escola de Engenharia de Lorena, University of Sao Paulo, 12602-810 Lorena, Brazil
[b] Instituto de Física, University of Sao Paulo, 05314-970 Sao Paulo, Brazil
[c] Karlsruher Institut für Technologie, D-72061 Karlsruhe, Germany
[d] Instituto de Física Rosario, CONICET-UNR, 2000 Rosario, Argentina

ARTICLE INFO

Article history:
Received 24 October 2015
Received in revised form
22 May 2016
Accepted 9 June 2016
Available online 11 June 2016

Keywords:
AISI 201 austenitic stainless steel
Strain induced martensite
Martensite reversion
Magnetic properties
Microstructural evolution

ABSTRACT

Strain-induced martensite (SIM) and its reversion in a cold-rolled AISI 201 austenitic stainless steel was studied by means of magnetic properties, light optical (LOM) and scanning electron (SEM) microscopy, electron backscatter diffraction (EBSD), texture measurements, and Vickers microhardness testing. According to Thermo-calc© predictions, the BCC phase (residual δ-ferrite and SIM) is expected to be stable until 600 °C. The current material was cold rolled up to 60% thickness reduction and submitted to both isothermal and stepwise annealing up to 800 °C. Magnetic measurements were taken during annealing (*in situ*) of the samples and also for their *post mortem* conditions. The Curie temperatures (T_c) of residual δ-ferrite and SIM have similar values between 550 and 600 °C. Besides T_c, the focused magnetic parameters were saturation magnetization (M_s), remanent magnetization (M_R), and coercive field (H_c). SIM reversion was found to occur in the range of 600–700 °C in good agreement with Thermo-calc© predictions. The microstructures of the material, annealed at 600 and 700 °C for 1 h, were investigated via EBSD. Microtexture measurements for these samples revealed that the texture components were mainly those found for the 60% cold rolled material. This is an evidence that the SIM reversion occurred by an athermal mechanism.

1. Introduction

Austenitic stainless steels have been extensively studied due to their good corrosion resistance, good formability and toughness [1,2]. The combination of these properties makes this class of steels very attractive for nuclear and chemical processing applications [3].

Upon straining, metastable austenite transforms into martensite in austenitic stainless steels, the so-called "strain-induced martensite" (SIM). It was found that SIM nucleates at shear bands intersections that may be in the form of deformation twins or dense bundles of stacking faults [1,4,5]. Besides plastic strain, the amount of SIM depends on the chemical composition of the steel and working temperature [1]. Two different types of martensite can be formed: ε-martensite, with a hexagonal-close-packed (HCP) structure, and α'-martensite, with a body-centered-cubic (BCC) structure [6]. There is a large number of studies concerning strain-induced martensite in austenitic stainless steels, most of them related to conventional 300 series of steels [7–9]. According to many authors, the formation of ε-martensite occurs at a small strain and it transforms into α'-martensite at larger strains [10–13]. However, some authors claim that α'-martensite forms directly from austenite [14]. On the other hand, recent studies suggest that, depending on grain size, ε-martensite is or is not an intermediate phase in the α'-martensite [15,16].

According to the literature, martensite reversion can occur by two mechanisms during annealing, *i.e.* athermal or diffusion-controlled. In case of athermal mechanism the process occurs by means of coordinated movement of atoms. Hence, a correspondence between product and parent lattice exists. This allows the reverted austenite to maintain the same texture of cold-rolled austenite. On the other hand, in the diffusional mechanism there is a long-range rearrangement of atoms. Consequently, the correspondence between parent and product lattices is not observed anymore and the resulting texture can be random [17].

ε-martensite is paramagnetic as well as austenite (γ), while α'-martensite is ferromagnetic. Hence, magnetic measurement is a

* Corresponding author.
E-mail address: msandim@demar.eel.usp.br (M.J.R. Sandim).

http://dx.doi.org/10.1016/j.jmmm.2016.06.027
0304-8853/

powerful nondestructive technique for monitoring the bulk transformation $\gamma \rightarrow \alpha'$ during plastic deformation of austenitic stainless steels [6,12,18,19]. Saturation magnetization (M_s) is very often used to evaluate the volume fraction of martensite, since M_s is related to the amount of ferromagnetic phase in the material [18,20]. In comparison to M_s, fewer studies focused on the coercive field (H_c) behavior of deformed austenitic stainless steels followed by annealing [18]. Regarding such materials, this magnetic parameter can give information about the shape and distribution of martensite throughout the microstructure [6,18].

In consequence of rolling, texture develops and elongated grains appear in the material [21,22]. A textured polycrystalline material itself has a magneto-crystalline anisotropy dependent on the orientation components developed upon straining [20]. In addition, if the elongated grains belong to a ferromagnetic phase, shape anisotropy effects (arising from demagnetizing fields) also become important [20]. The combination of the anisotropic effects described above can lead to an easy axis of magnetization along the rolling direction [22]. Even concerning austenitic stainless steels a third kind of anisotropy can be relevant. It is well known that an important phenomenon related to magneto-elastic anisotropy deals with the effect of internal and or applied stress/or strain on the magnetization in a ferromagnetic specimen [20,23]. In austenitic stainless steels the generation of SIM is associated with strong internal stress fields. Therefore, we have to keep in mind a possible impact of magneto-elastic effect on the magnetic properties of such materials [20,23]. However, due to its complexity, the evaluation of such effect it is not an easy task and have not been considered in the present work.

The 200 series differs from the 300 series mainly by having a smaller Ni content [13,24]. Another important difference between these two steel grades is that the 200 series have a higher susceptibility to martensitic transformation [13]. In comparison with the traditional 300 series there are only a few works focusing SIM in AISI 201 steel [13,25–27]. The focus of this work is the study of SIM and its reversion in AISI 201 steel using both microstructural and magnetic characterization techniques. For this study, the steel was cold rolled up to 60% thickness reduction and annealed up to 1000 °C. *In situ* magnetic measurements taken during stepwise heating of the samples were compared to those obtained for the same samples in their *post mortem* condition (after air cooling down to room temperature). Magnetic measurements at room temperature were also taken for the samples isothermally annealed in the same temperature range. In addition to magnetic measurements, samples were also characterized using quantitative metallography, Vickers microhardness testing, light optical and scanning electron microscopies (LOM and SEM), and Electron Backscatter Diffraction (EBSD). The analysis of the obtained results was complemented using thermodynamic calculations (Thermo-calc©).

2. Experimental methods

2.1. Material and thermodynamic simulations

The nominal chemical composition of the AISI 201 steel is presented in Table 1. This material, supplied by Aperam South America (Brazil), was solution annealed in the temperature range 1050–1150 °C for about 30 s. Based on the chemical composition, thermodynamic calculations were performed for the annealing temperatures used in this work, by Thermo-calc© software coupled with TCFE7 database (see Section 2.3).

Table 1
Chemical composition of AISI 201 steel (%wt).

C	Mn	Si	Cr	Ni	Mo	Cu	N	Al
0.0237	7.018	0.382	17.06	4.07	0.0429	0.0717	0.1640	0.0047

2.2. Cold rolling and microstructural characterization

A 3-mm thick plate was cold rolled up to 60% thickness reduction (or to an equivalent strain to $\varepsilon = 0.916$) in multiple passes. After conventional grinding, samples of the *as-received* material were submitted to electrolytic polishing in a solution of sulfuric acid (20% vol) and methanol, at 12 V for 15 s. In addition, the material was submitted to electrolytic etching using an aqueous NaOH solution (40% vol) at 5 V for 30 s to allow the visualization of δ-ferrite. The volume fraction of δ-ferrite was calculated using Image-J software using digitalized images obtained by light optical microscopy (LOM). After that, the material was submitted to electrolytic etching using a solution of oxalic acid (10% vol) at 3 V for 30 s. New images via LOM were acquired and the mean austenitic grain size was estimated by means of quantitative metallography. The samples obtained from the cold-rolled material (20%, 40%, and 60% of thickness reduction) were only etched with oxalic acid solution (10% vol, at 3 V for 30 s).

Representative samples were characterized using EBSD. In this case, the sample preparation involved conventional grinding and polishing, followed by an electrolytic polishing in a solution of sulfuric acid (20%vol) and methanol using a voltage of 12 V for 15 s. For the EBSD mappings, a Zeiss Merlin microscope was operated at 20 kV, coupled with an EBSD system with an Edax Hikari high-speed camera. Maps with $50 \times 50\ \mu m^2$ were acquired with a step size of 40 nm. The obtained raw data were analyzed using TSL-OIM analysis software. For cleanup procedure, standard EBSD data cleanup techniques were used including neighbor CI (confidence index) correlation and grain dilation with a grain tolerance of 5° and a minimum grain size of 10 pixels. All points containing CI below 0.1 were removed from the maps.

For macrotexture characterization of the 60% cold rolled material, one sample was taken from the plate and ground up to half thickness reduction. The surface perpendicular to the normal direction (ND) was polished and the macrotexture measurements were performed in this sample using a texture goniometer MPD Philips with Cu-Kα radiation (40 kV, 30 mA). The data obtained were analyzed using popLA© software. In addition to microstructural characterization, Vickers microhardness testing was performed on the longitudinal sections of polished samples using a load of 200 g for 30 s.

2.3. Magnetic measurements

For the magnetic characterization, samples were cut using a low-speed diamond wheel saw. Four different sets of samples were investigated as following:

i) Hysteresis loops at room temperature were obtained for samples with 0%, 20%, 40%, and 60% thickness reduction using a vibrating sample magnetometer (VSM) from EG&G Princeton Applied Research. For these measurements, the samples were cut into $1 \times t \times 5\ mm^3$ approximate dimensions, where t is the thickness of the plate and the larger dimension (5 mm) is parallel to the rolling direction (RD). The field was applied parallel to the RD.
ii) *In situ* magnetization measurements were performed during stepwise heating of the samples ($\varepsilon = 0.916$) from room temperature up to 800 °C, under flowing Ar, using a VSM Lakeshore Model 7404. The heating rate until a particular target temperature was 3 °C/min. After stabilization (15 min), the

tracing of a complete hysteresis loop required 14.7 min, so that for each target temperature the sample was annealed during ~30 min. Starting from room temperature, the chosen target temperatures were: 200, 300, 400, 500, 600, 700, and 800 °C. For these measurements two $4 \times 2 \times 1.2$ mm^3 samples were cut, with the larger dimension taken at two conditions, viz. parallel and perpendicular to the RD, respectively. Magnetization curves were carried out with the external field parallel to the larger dimension of the sample (4 mm), in order to obtain the hysteresis loops for two field configurations, i.e, the magnetic field (H) applied either parallel (//RD) or perpendicular to the RD (⊥RD). Additional four samples ($\varepsilon = 0.916$) were submitted to the heating cycles described above for field configuration H//RD. In this case, these four samples were retrieved from the system after the completion of all cycles up to 500, 600, 700, and 800 °C. These samples were labeled as piece 1, 2, 3, and 4, respectively. All the samples were furnace cooled, under flowing Ar. Hysteresis loops were taken for these four samples after cooling down to room temperature (*post mortem* condition).

iii) Further *in situ* magnetization measurements were carried out for both *as-received* and cold rolled ($\varepsilon = 0.916$) materials. For each condition, two samples were cut according to the protocol described in item (ii). The first sample was obtained by means of conventional cutting (using low-speed diamond saw). However, the second one was deeply etched in *aqua regia* solution for 60 s after cut. These four samples were submitted to magnetization measurements taken in the presence of a fixed external magnetic field (H//RD), in the temperature range 25–1000 °C, for a heating rate of 3 °C/min. The external magnetic field was ~90 Oe and ~115 Oe for the *as-received* and cold rolled ($\varepsilon = 0.916$) samples, respectively. These magnetic fields promote a magnetization (M) equal to 10% of M_s in each correspondent sample.

iv) Samples ($\varepsilon = 0.916$) were cut according to item (i) and isothermally annealed in vacuum (sealed in quartz glass tubes) in a resistive furnace. Annealing was performed at several temperatures in the range 200–800 °C for several times up to 180 min, followed by air-cooling. For these annealed samples, hysteresis loops were obtained at room temperature, using the same protocol described above. The isothermal annealing temperatures described above are indicated as "T_a" in the corresponding graphics (Section 3.3).

Coercive field (H_c), saturation magnetization (M_s), and remanent magnetization (M_R) were obtained from the hysteresis loops of the samples with an accuracy of ±5 Oe, 2%, and 2%, respectively.

3. Results and discussion

3.1. As-received and deformed conditions

The steel in the *as-received* condition is fully-recrystallized and it does not contain deformation twins in the microstructure. The mean austenitic grain size is 17 ± 6 μm. In addition, it was observed the presence of elongated islands of δ-ferrite in the microstructure, a residual phase very often found in commercial austenitic stainless steels, pinned during the solidification [28]. From the analysis of 15 different regions chosen by chance in the microstructure, the volume fraction of δ-ferrite in the *as-received* material was 2.0 ± 0.8%.

Fig. 1(a) shows the Thermo-calc© predictions for the stable phases (in terms of volumetric fraction) as a function of temperature. From this figure, the BCC phase (ferrite) is expected to be

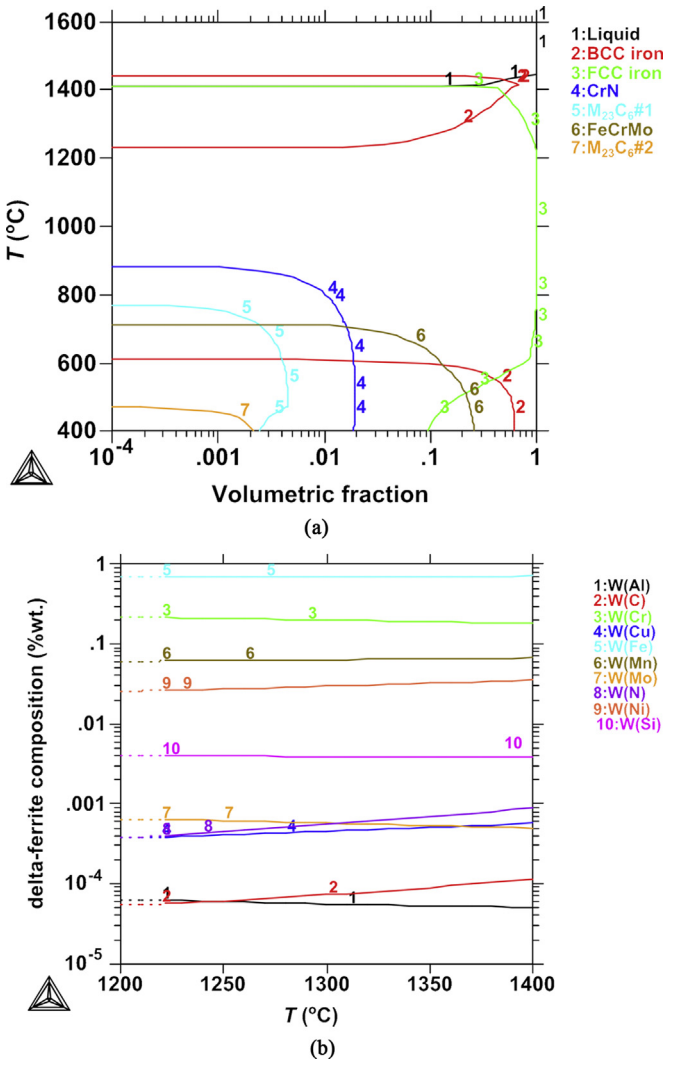

Fig. 1. Thermo-calc© simulations for AISI 201austenitic stainless steel: (a) volume fraction of the phases and (b) chemical composition of δ-ferrite as a function of temperature.

stable until 600 °C, *i.e.* there is no dissolution of this phase for annealing temperatures lower or equal to 600 °C. In this context, although δ-ferrite is a residual phase in this material, it is plausible to infer that it is stable until 600 °C. Therefore, based on Fig. 1(a) it is also assumed that the chemical composition of δ-ferrite is the one found at T ~1220 °C. This temperature corresponds to the lowest temperature where δ-ferrite would be present in the microstructure during solidification. The correspondent chemical composition of δ-ferrite predicted by Thermo-calc© is indicated in Fig. 1(b).

In the *as-received* condition, the steel presents a magnetic signal, as displayed in Fig. 2. This figure shows two curves of magnetization. One of them is the raw data of $M(H)$. Note that this curve does not reach the saturation due to the paramagnetic contribution of austenite. By taking the linear fit of the last portion of this curve (as indicated in Fig. 2), we can find an equation of a straight line passing through the origin, with the same slope. Such straight line can approximately represent the paramagnetic contribution to $M(H)$. Once this contribution is subtracted from the raw data, we obtain the second curve displayed in Fig. 2, which reaches saturation. Since the *as-received* material has a small fraction of δ-ferrite, it is plausible to assume that the magnetic signal of the *as-received* material comes from this phase. According to Merinov et al. [29], the amount of δ-ferrite in austenitic

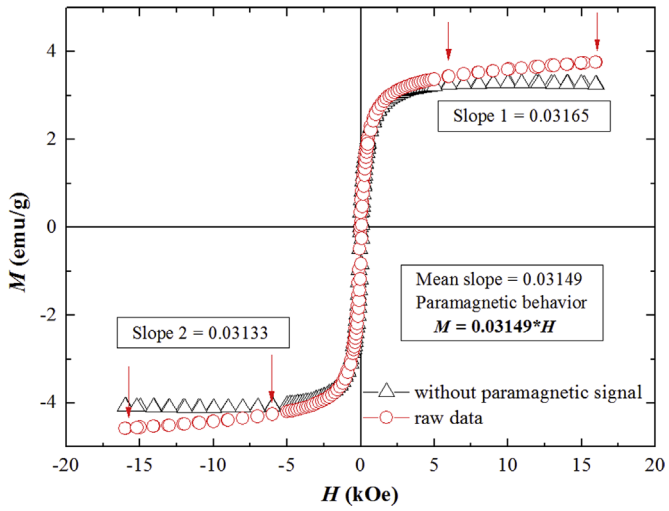

Fig. 2. Magnetization curve taken at room temperature for the steel in the *as-received* condition: the red curve represents the raw data and the black one is the same curve without the paramagnetic contribution. Arrows indicate the last portions of the raw curve used to find the slope that rules the paramagnetic contribution. (For interpretation of the references to color in this figure legend, the reader is referred to the web version of this article.)

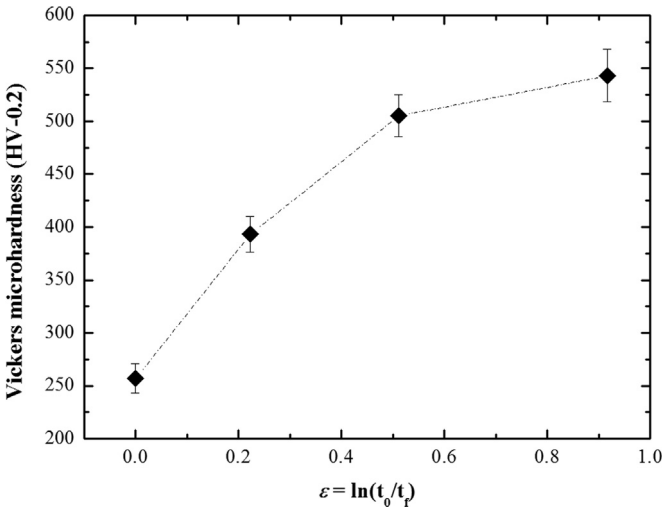

Fig. 3. Work hardening behavior of AISI 201 austenitic stainless steel.

stainless steel can be calculated using Eq. (1), as follows:

$$\%\delta = \frac{4\pi I}{4\pi I_\delta} \cdot 100 \quad (1)$$

where $4\pi I$ (tesla) corresponds to the saturation magnetization of the sample containing δ-ferrite. The term $4\pi I_\delta$ (tesla) is the saturation magnetization of the δ-ferrite and it is given by the following empirical formula in terms of its chemical composition [29]:

$$4\pi I_\delta = 2.1 - 0.0275\%Cr - 0.0330\%Ni - 0.0260\%Mo - 0.0670\%Ti - 0.0610\%Si - 0.0630\%Al - 0.0600\%V - 0.0280\%Mn \ (\text{Tesla}) \quad (2)$$

From $M(H)$ measurements based on four samples of the *as-received* material, and using the protocol displayed in Fig. 2, the M_s value of the *as-received* material is in average 3.8 emu/g. Such value corresponds to $4\pi I = 0.033$ T. Using the data for the δ-ferrite chemical composition as predicted by Thermo-calc© (see Fig. 1 (b)), from Eq. (2) the $4\pi I_\delta$ value is 1.17 T. Using the Eq. (1), the estimated amount of δ-ferrite in the *as-received* material is $2.8 \pm 0.1\%$, which is in very good agreement with the value obtained from quantitative metallography. This result also supports that there is no SIM in the *as-received* material, as inferred from its metallographic examination.

The work hardening behavior of this steel is displayed in Fig. 3. From this figure, it was observed that the hardness increased more rapidly up to a low strain ($\varepsilon = 0.223$) and the hardness increase rate became progressively lower until the maximum deformation was reached. Baldo and Mészáros [30] reported a similar result in lean duplex stainless steel, which also experiences strain-induced martensite transformation. According to these authors, work hardening of austenite occurs even at low strains. With increasing rolling reductions, SIM becomes the principal mechanism of strain accommodation, which leads to a progressive decrease in the slope of the work hardening curve (as seen in Fig. 3).

Images of the samples deformed up to 20% and 60% thickness reduction are depicted in Fig. 4(a) and (b), respectively. For the lower strain, the microstructure consists of rather equiaxed austenitic grains and deformation twins. It must be emphasized that, according to the references [12,31,32], the intersection of

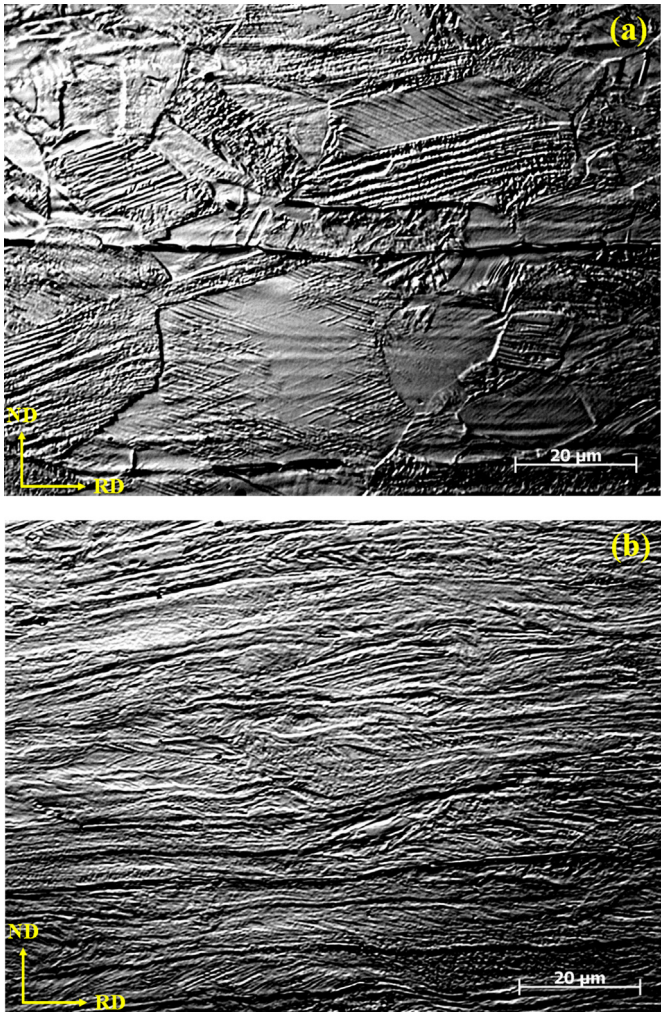

Fig. 4. Light optical micrographs of AISI 201 austenitic stainless steel after cold rolling: (a) 20% and (b) 60% thickness reduction (Nomarski contrast).

deformation twins is a preferential site for nucleation of SIM. In addition, it can be noticed the presence of elongated islands of δ-ferrite parallel to the RD. For the 60% cold-rolled condition (Fig. 4 (b)) the microstructure consists of elongated grains aligned with the RD. Deformation twins, shear bands as well as S-bands are

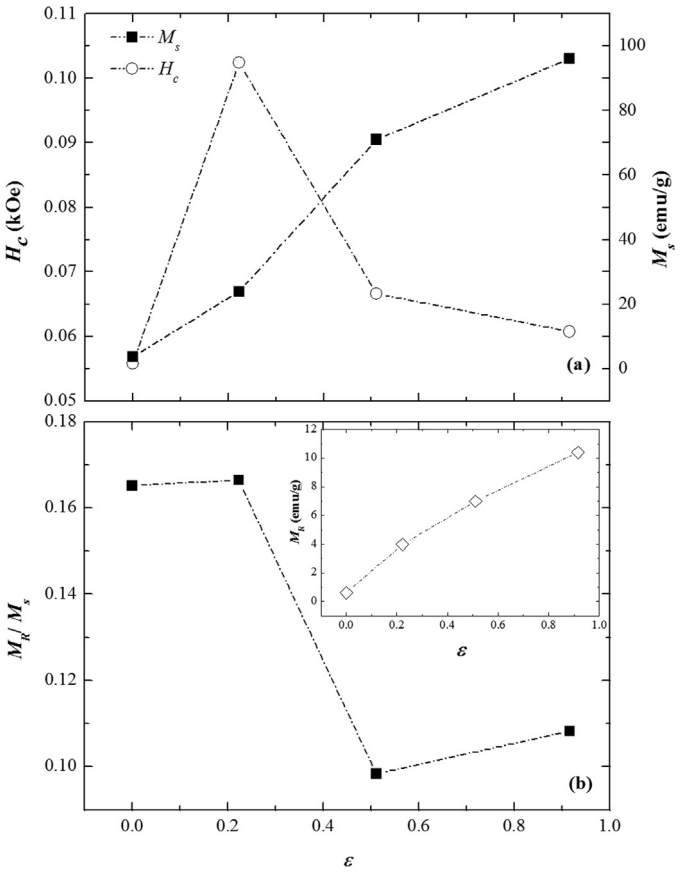

Fig. 5. (a) Saturation magnetization (M_s) and coercive field (H_c) of AISI 201 austenitic stainless steel, cold rolled up to 60% thickness reduction and (b) correspondent M_R/M_s values in function of true strain. In the inset of (b) is shown the linear behavior of remanence in function of strain.

visualized in the microstructure. Concerning the macrotexture analysis (not shown) of 60% cold-rolled AISI 201 steel, it was found that the main texture components of the remaining austenite are $\{011\}<001>$ Goss, $\{011\}<211>$ Brass, $\{112\}<111>$ Copper, and $\{123\}<634>$ S. On the other hand, the main texture components for α'-martensite are rotated cube $\{001\}<011>$, α and γ fibers. Other references report similar texture components for cold-rolled austenitic stainless steels [17,33,34].

Fig. 5(a) shows both the M_s and H_c values for the AISI 201 steel cold rolled up to 60% thickness reduction. Concerning the M_s behavior in this figure, we see a progressive increase of M_s with deformation, as a clear indication of SIM. According to Mumtaz et al. [6], the $M_s = 154$ emu/g for 100% α'-martensite. On the other hand, the corresponding value obtained by Tavares et al. [13] for a modified 201 steel with similar composition is 140 emu/g. From the M_s data displayed in Fig. 5(a) and using the values of M_s for 100% α' martensite phase reported in the literature [6,13], the martensite volume fraction of the investigated steel cold rolled up to 60% thickness reduction is 60–65%. It must be pointed out that, in this estimation, the magnetic signal coming from δ-ferrite was subtracted. Concerning the coercive field, Fig. 5(a) shows that H_c presents a high value for 20% thickness reduction, followed by a noticeable drop with the increase in deformation. For austenitic stainless steels, the coercive field is strongly dependent on size, shape, and distribution of martensite [3,6,18]. According to some authors [3,18] the peak behavior of H_c can be attributed to pinning effects of the magnetic domain walls by the α'/γ interfaces. However, the most probable phenomenon that rules behavior of H_c in austenitic stainless steels is the shape magnetic anisotropy [20,23], as reported by Mumtaz et al. [6]. They argue that, when the volume of α'-martensite phase is small, it has a strong shape magnetic anisotropy and, consequently, its coercive force is large [6]. Therefore, when the coalescence of the martensite phase occurs (with further deformation), such magnetic anisotropy decreases, as well as H_c [6]. Back to the Fig. 5(a), in light of Ref. [6] we can infer that, up to 20% thickness reduction, the size of the SIM laths i**s** quite small, so that α'-martensite phase has a strong shape magnetic anisotropy. With further deformation, coalescence of the martensite occurs, leading to a decrease of H_c. From Fig. 5(a) note that the highest increase percentage of M_s occurs between 20% and 40% thickness reduction. The strongest reduction of H_c occurs at the same deformation range, as depicted in the same figure. Back to Fig. 3, also for this specific deformation range, a slight decrease in the slope of hardness curve is observed. As previously discussed, such slight decrease in the slope of hardness is due to SIM transformation.

It is known that the remanence is the ability of a material to retain magnetization. Indeed, the ratio M_R/M_s (also called squareness ratio) measures how "square" a given hysteresis loop is [20]. Regarding the present work, it was found a linear increase of the remanence with strain (see the inset of Fig. 5b). The main panel of Fig. 5(b) shows the behavior of M_R/M_s ratio as function of strain. Note that there is an evident decrease in the M_R/M_s ratio between 20% and 40% thickness reduction. For the same strain range, it was observed the largest decrease in H_c, as depicted in Fig. 5(a). According to ref. [6], the results displayed in Fig. 5 suggest that the pronounced decrease in M_R/M_s ratio also mirrors a decrease in the shape magnetic anisotropy of α'-martensite phase in the strain range 0.2–0.5. However, we have to keep in mind that the evolution of the M_R/M_S ratio can possibly be affected by magneto-elastic effects (Villari effect) [20].

3.2. Cold-rolled AISI 201 steel with further stepwise annealing

For a fixed applied field parallel to the RD, Fig. 6(a) and (b) show the temperature dependence of magnetization $M(T)$ of the *as-received* and 60% cold-rolled samples, respectively. In both figures (a) and (b), two curves of $M(T)$ are displayed as well as their derivatives (see the insets). One of them is related to the sample cut in a conventional way (black line). The second one corresponds to the sample which was deeply etched after cutting (red line). From Fig. 6(a) and (b) there are no substantial differences between the two displayed $M(T)$ curves. Therefore, we can safely assume that SIM due to the sample-cutting process adopted in the present investigation is negligible and, in addition, that the magnetic signal in the *as-received* material is due to δ-ferrite. Concerning the *as-received* material, Fig. 6(a) shows that magnetization presents a noticeable drop around 550 °C, as evidenced in the inset of this figure. So, we can also infer that the Curie temperature of δ-ferrite is ~550 °C. It must be stressed that, according to Thermo-calc© predictions, the residual δ-ferrite is expected to be stable until 600 °C. Concerning the 60% cold-rolled steel, from Fig. 6(b) it is observed that the magnetization decreases progressively with temperature until a sharp drop to zero in the range 550–600 °C, as evidenced in the inset of this figure. These results suggest that the reversion of the SIM occur between 550 and 600 °C. Furthermore, the sharp drop to zero observed for magnetization can be related to the Curie temperature of the remaining martensite. It must be stressed that the amount of carbon in the investigated steel is low and, in consequence, the structure of martensite is expected to be BCC [35]. Therefore, since δ-ferrite and SIM are BCC, according to Fig. 6(a) and (b), they have practically the same Curie temperature, *i.e.* in the range 550–600 °C.

In situ $M(H)$ curves obtained for 60% cold-rolled AISI 201 steel annealed up to 800 °C with the magnetic field applied parallel to the RD (not shown), revealed a ferromagnetic behavior up to

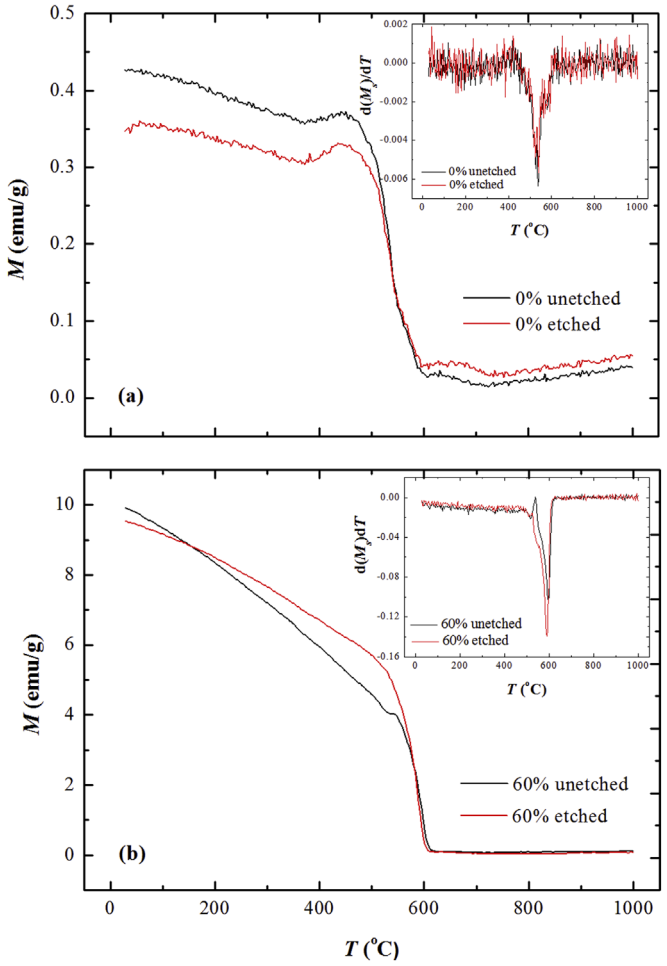

Fig. 6. Temperature dependence of magnetization for AISI 201 steel for (a) *as-received* condition with an applied field $H \sim 90$ Oe (H//RD) and (b) 60% cold-rolled with $H \sim 115$ Oe (H//RD). In both (a) and (b) figures two $M(T)$ curves are displayed. They correspond to the sample taken without and with deep etching in *aqua regia* after cutting, respectively. The insets show the correspondent d$M(T)$/dT curves in function of temperature. (For interpretation of the references to color in this figure, the reader is referred to the web version of this article.)

500 °C. For higher temperatures such behavior disappears and the $M(H)$ curves show a paramagnetic response. A similar behavior was observed for the *in situ* $M(H)$ curves obtained with field perpendicular to RD (not shown). Such paramagnetic behavior for temperatures higher than 500 °C is a combination of two factors: reversion of the SIM takes place and the Curie temperature of both δ-ferrite and remaining α'-martensite is reached.

Fig. 7 shows both H_c and M_s values obtained from *in situ* hysteresis loops of the two samples annealed up to 500 °C for the two conditions of applied field (for one of them H//RD and for the other one $H\perp$RD). Both H_c and M_s decrease with temperature, possibly due to relaxation of magneto-crystalline constants with increasing temperature [20]. Concerning H_c behavior, Mumtaz et al. [6] claimed that H_c depends on the magnetization direction in cold-rolled austenitic stainless steels. However, for the investigated material in this work, from the main panel of Fig. 7 we see that there are no major differences between the H_c values for H//RD and $H\perp$RD. ElMassalami et al. [22] reported about an angular dependence in M_s related to the RD for a superduplex steel. In Ref. [22] such effect was attributed to a magnetic anisotropy induced by rolling. However, in the present work the M_S values are almost the same for both field configurations (H//RD and $H\perp$RD), as displayed in the inset of Fig. 7.

To going deeper in the magnetic behavior we have performed

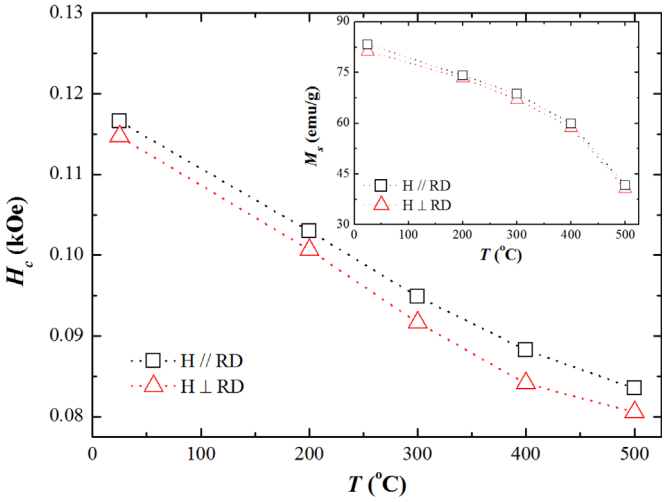

Fig. 7. H_c (in the main panel) and M_s (in the inset) values for both conditions of applied field, obtained from *in situ* hysteresis loops taken at several temperatures up to 500 °C for 60% cold-rolled AISI 201 steel.

additional experiments for H//RD. Four additional samples were submitted to the same annealing process above described. However, these four samples were retrieved from the furnace after finishing the cycle up to 500, 600, 700, and 800 °C, respectively. As previously described in Section 2.3 (ii), these samples were labeled as piece 1, 2, 3, and 4, respectively. After cooling, $M(H)$ curves were taken at room temperature for these samples. The H_c and M_s values obtained in their *post mortem* condition are displayed in Fig. 8

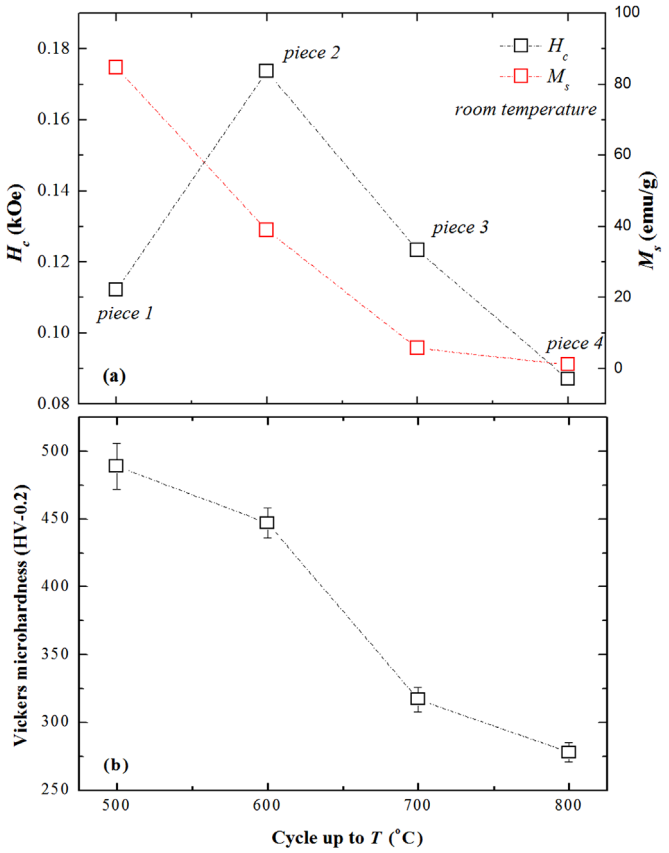

Fig. 8. (a) H_c and M_s values (taken at room temperature, after furnace cooling) and (b) corresponding Vickers microhardness of the samples of AISI 201 steel (60% thickness reduction) submitted to stepwise heating up to 500, 600, 700 and 800 °C (pieces 1, 2, 3, and 4, respectively). (For interpretation of the references to color in this figure legend, the reader is referred to the web version of this article.)

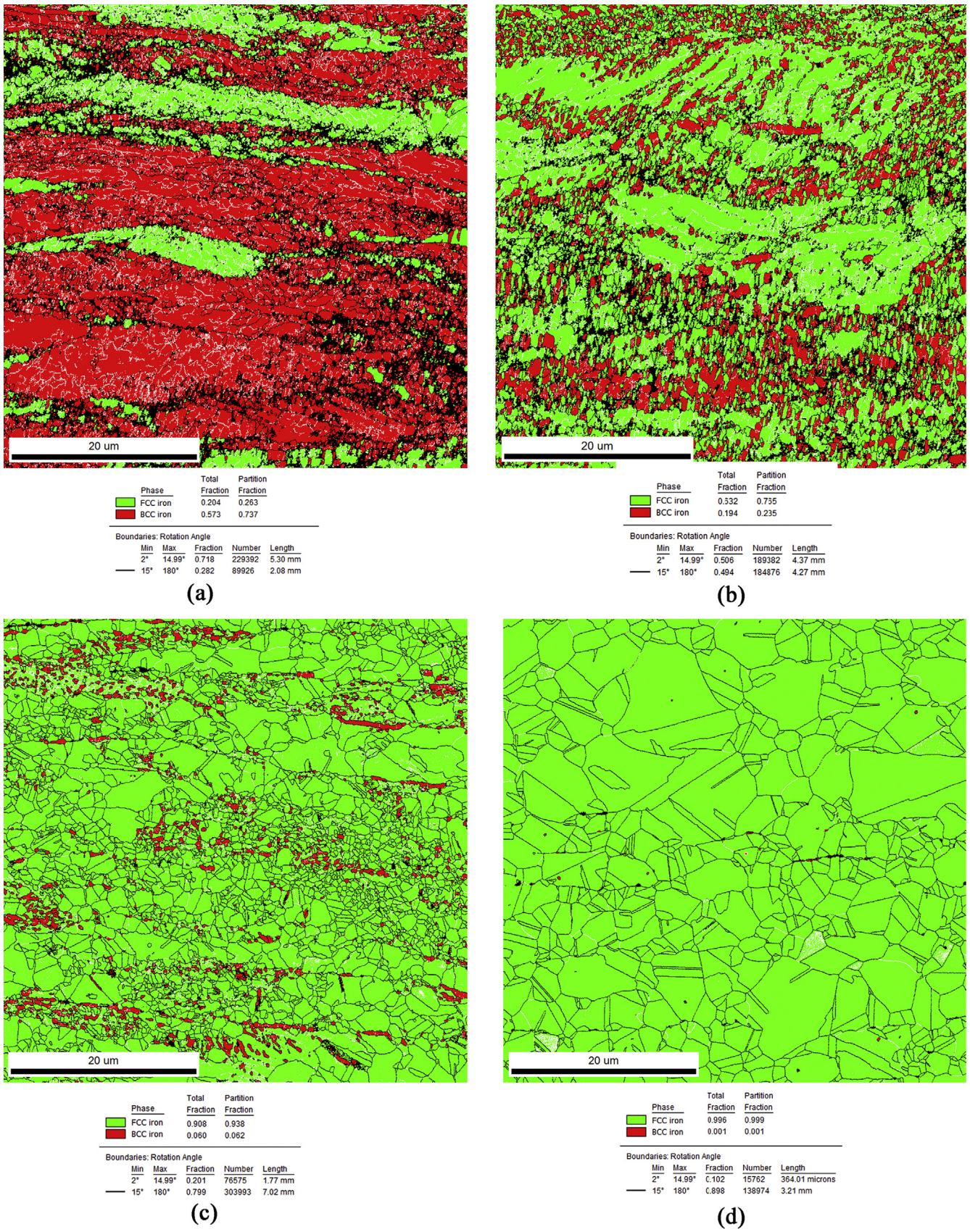

Fig. 9. EBSD phase maps of the samples of AISI 201 steel (60% thickness reduction) submitted to stepwise heating up to (a) 500, (b) 600, (c) 700 and (d) 800 °C. (For interpretation of the references to color in this figure legend, the reader is referred to the web version of this article.)

(a). From this figure, in correspondence to a noticeable decrease of M_s with increasing temperature between 500 and 700 °C there is an evident peak in H_c behavior, with maximum at 600 °C. Due to reversion of martensite there is an increase in the number of martensite/austenite boundaries. In consequence of such fragmentation of the martensite phase, the ferromagnetic particles become less connected. So, as discussed before, the peak behavior observed in Fig. 8(a) can also be attributed to a strong increase of local demagnetizing fields (shape magnetic anisotropy) [6,23]. For samples annealed at temperatures higher than 600 °C, in consequence of the shrinkage of the martensite regions, H_c decreases to a minimum value. Such peak behavior is not observed from the *in situ* magnetization measurements probably due to relaxation of the magneto-crystalline anisotropy constants with temperature. Fig. 8(b) shows the softening behavior for the same samples whose magnetic parameters are depicted in Fig. 8(a). From this figure, it is observed that the hardness values decrease continuously but the highest amount of softening (~33%) occurs between 600 and 700 °C.

Fig. 9 shows the microstructure of the same samples whose magnetic and softening behaviors are reported in Fig. 8(a) and (b), respectively. For the sample retrieved from the furnace at 500 °C (piece 1), from Fig. 9(a) there is no evidence of martensite reversion. On the other hand, martensite reversion is evident in the sample annealed up to 600 °C, piece 2 (Fig. 9(b)). In this figure, very fine austenite grains are found within the martensite structure. Consequently, martensite also becomes refined leading to the maximum number of austenite/martensite boundaries. Such microstructural configuration leads to the maximum value of H_c observed in Fig. 8(a). From Fig. 9(b) it is also possible to see the presence of large austenitic areas aligned to the RD. These regions correspond probably to untransformed austenite during cold rolling. Such untransformed austenite then underwent recovery during *in situ* magnetic measurements between 500 and 600 °C. Thus, both reversion of martensite and recovery of untransformed austenite are responsible for the slight decrease in hardness between 500 and 600 °C observed in Fig. 8(b). From Fig. 9(c), in comparison to samples annealed up to lower temperatures, a noticeable difference is found for the sample annealed up to 700 °C (piece 3). At this temperature, a mixture of fine and coarser austenite grains is observed. The remaining martensitic structure (~6%) is much more refined than the previous ones observed in Fig. 9(a) and (b). Surrounding this fine martensite there are fine austenite grains that are able to grow since austenite does not consume martensite. Probably that is the reason why the reverted austenite grains at 700 °C are larger than those ones observed at lower temperatures. From Fig. 9(c) it is also noticeable the presence of larger recrystallized austenite grains. These grains are consequence of recrystallization of the austenite that did not experience martensitic transformation during deformation. The combination of discontinuous recrystallization and growth of reverted austenite explains the highest decrease of hardness between 600 and 700 °C depicted in Fig. 8(b). Finally, Fig. 9(d) shows that the microstructure of the sample annealed up to 800 °C (piece 4) is practically austenitic and the fraction of α'-martensite is negligible. It also must be noticed that the tiny red regions in this figure can be δ-ferrite. It corroborates the low value of M_s found for this sample (see Fig. 8(a)). Besides, the hardness value of this sample (see Fig. 8(b)) is close to the correspondent value of the *as-received* material.

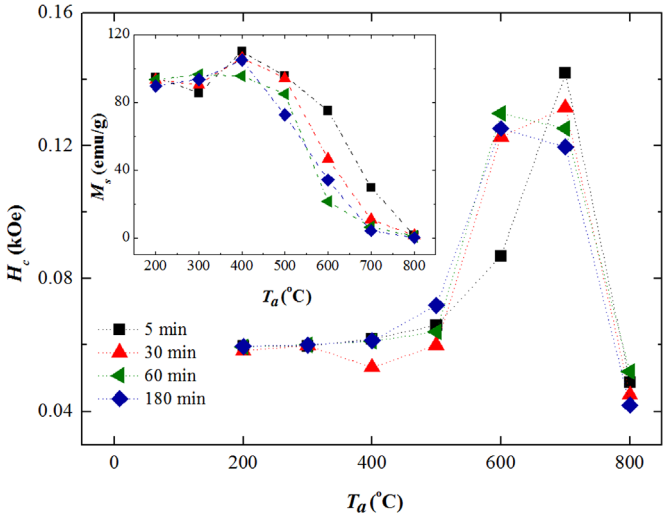

Fig. 10. H_c (in the main panel) and M_s (in the inset) values of 60% cold-rolled AISI 201 steel isothermally annealed up to 800 °C for several annealing times. Both values of M_s and H_c were obtained from the hysteresis loops taken at room temperature (H//RD).

3.3. Cold-rolled AISI 201 steel (60%) with further isothermal annealing

In order to complement the analysis reported in Section 3.1 we have also performed several isothermal annealing treatments in 60% cold-rolled samples, as described in Section 2 (item iv). From the hysteresis loops of these samples taken at room temperature (not shown), we have obtained their correspondent values of M_s, H_c and M_R. Fig. 10 shows both the values of H_c and M_s for samples isothermally annealed from 200 to 800 °C ("T_a") for annealing times varying from 5 to 180 min. From the inset of Fig. 10 it is observed a slight increase of M_s between 300 and 400 °C, followed by a noticeable decrease of M_s at higher temperatures. According to Padilha et al. [1], the slight increase of M_s before the martensite reversion in austenitic stainless steels is probably due to static recovery mechanisms occurring at low annealing temperatures. Such mechanisms cause stress relieving around the martensite laths, which can experience an additional growth just before reversion. Regarding the coercive field, from the main panel of Fig. 10 we see that H_c keeps around the same value from 200 to 500 °C, independently of annealing time. For temperatures higher than 500 °C, H_c presents a strong increase until 600–700 °C, with further decrease to a minimum value at 800 °C. Such peak behavior of H_c is similar to one previously described regarding Fig. 8(a).

M_R/M_s ratio values as function of annealing times at four

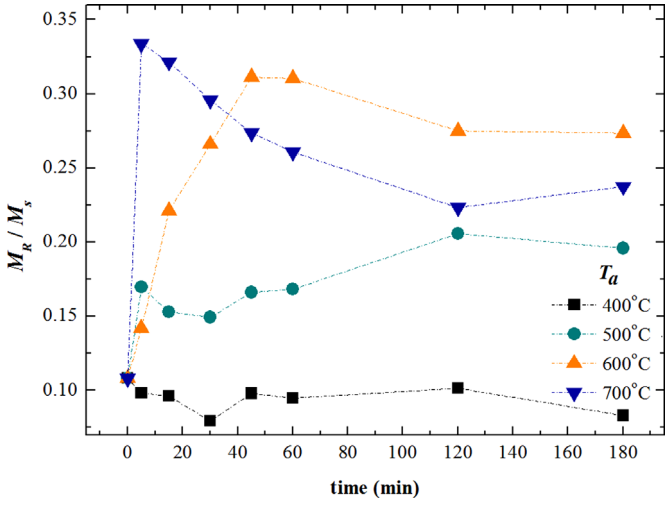

Fig. 11. The squareness M_R/M_s ratio (at room temperature) as a function of annealing time at 400, 500, 600 and 700 °C for 60% cold-rolled AISI 201 steel.

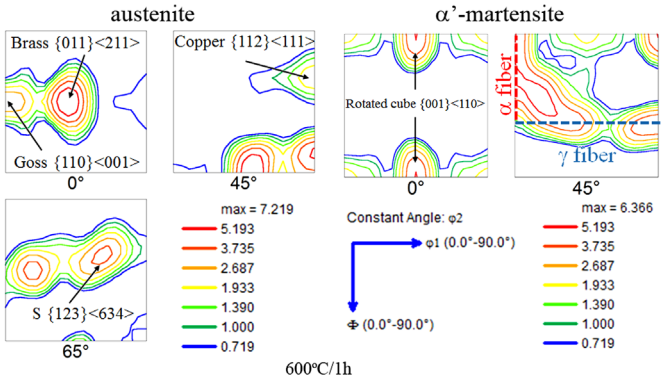

Fig. 12. Orientation distributions functions (ODF) from EBSD data for 60% cold-rolled AISI 201 steel annealed for 1 h at 600 °C. (For interpretation of the references to color in this figure legend, the reader is referred to the web version of this article.)

representative temperatures can be seen in Fig. 11. In correspondence to the peak behavior of H_c displayed in Fig. 10 at temperatures 600–700 °C, we observe high values of M_R/M_s at the same temperatures. We also observe a sharp increase in the M_R/M_s value at 700 °C for a very short annealing time. Such increase corresponds to the fragmentation of the martensitic phase due to its reversion. A similar but no so sharp increase of M_R/M_s ratio is also observed for annealing at 600 °C. It is clear that drastic changes in the microstructure occurs in the first 40 min of annealing at 600 °C and in much lower annealing time at 700 °C.

The microtexture data for the sample annealed at 600 °C for 1 h is displayed in Fig. 12. This figure shows the orientation distribution functions (ODF) of austenite and α'-martensite and only representative ϕ_2=constant sections are depicted. Concerning the austenite phase note that the data displayed in Fig. 12 comes, without any distinction, from both reverted austenite and recovered austenite (which did not transform into martensite during deformation). For such annealing condition, it was observed that austenite keeps the same texture components found in 60% cold-rolled material (Goss, Brass, Copper, and S). Concerning α'-martensite, all cold rolling texture components (rotate cube, α and γ fibers) are present, although weaker. Literature reports that SIM reversion mechanism can be evaluated by texture measurements [17,36,37]. The above-described data for sample annealed at 600 °C for 1 h (which is in an earlier stage of SIM reversion) show

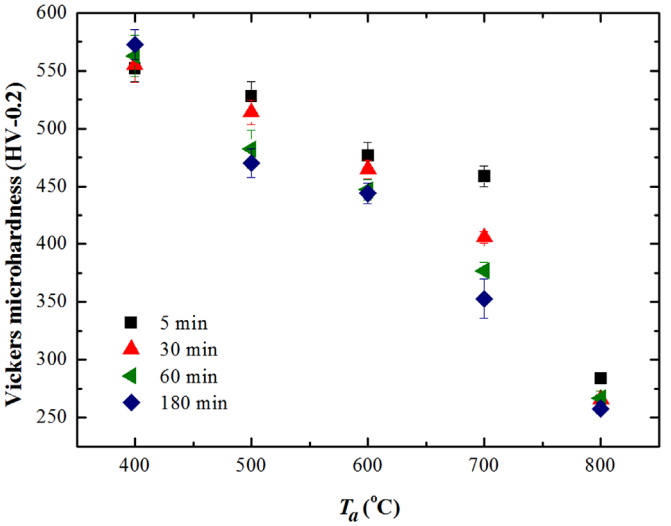

Fig. 13. Softening behavior of 60% cold-rolled AISI 201 steel isothermally annealed in the range 400–800 °C for times up to 180 min.

that austenite keeps the same texture of cold-rolled austenite. In the light of literature [17,36,37] such behavior suggests that SIM reversion occurs mainly by means of the athermal mechanism.

Fig. 13 shows the softening behavior for the same samples whose magnetic parameters are depicted in Fig. 10. Note that there is a sharp softening between 700 and 800 °C, likewise it is observed for H_c at the same temperature range. Besides, the hardness of the samples annealed at 800 °C for several time intervals are in accordance with the hardness of the *as-received* condition. These results indicate that the material becomes fully-recrystallized at 800 °C.

4. Conclusions

The microstructural evolution and the magnetic properties of AISI 201 austenitic stainless steel during cold rolling up to 60% thickness reduction followed by annealing up to 1000 °C were investigated. The following conclusions can be drawn:

1) The *as-received* material is fully recrystallized and it contains about 2% of δ-ferrite, which causes a small ferromagnetic signal. The Curie temperature of this minor phase is about 550 °C.
2) With increasing strain, deformation twins and shear bands can be noticed in the microstructure. The saturation magnetization increases indicating the occurrence of SIM. The highest increase percentage of M_s occurs between 20% and 40% thickness reduction. For the maximum thickness reduction (60%), the amount of martensite is 60–65%. H_c increases with strain up to 20% thickness reduction and presents a noticeable drop at higher strain. In correspondence to this drop in the magnitude of H_c, a sharp decrease in the ratio M_R/M_s is also observed. These results suggest the coalescence of martensitic regions at thickness reductions higher than 20%.
3) With aid of Thermo-calc© predictions, the BCC phase (residual δ-ferrite and SIM) is expected to be stable until 600 °C. It suggests that both residual δ-ferrite and SIM can be dissolved and reverted, respectively, at temperatures higher than 600 °C.
4) From *in situ* magnetic measurements of 60% cold-rolled samples, the reversion of strain-induced martensite occurs between 550 °C and 600 °C. At a given temperature, different samples presented similar values of H_c as well as M_S, independently of the field configuration, *i.e.*, parallel or perpendicular to the RD.
5) After cooling to room temperature, the H_c values of stepwise heated samples present a peak behavior, in correspondence to a pronounced decrease in M_s. The maximum value of H_c is found for the sample annealed up to 600 °C. Such peak behavior of H_c indicates that during reversion, martensite regions become progressively smaller and isolated, as supported by EBSD results. Shape magnetic anisotropy effects become stronger with increasing number of α'/γ interfaces leading to the increase of H_c.
6) Such peak behavior is not observed during *in situ* measurements probably due to relaxation of the magneto-crystalline anisotropy constants with temperature.
7) For 60% cold-rolled samples with further isothermal annealing a progressive decrease of M_s starts at about 500 °C. H_c presents a peak behavior in the range 500–800 °C and reaches its maximum at 600 or 700 °C, depending on the annealing time. These results are similar to the ones found for the stepwise annealed samples in the *post mortem* condition. In correspondence to the peak behavior in H_c, an increase in the M_R/M_s ratio was also verified. Both characteristics of H_c and M_R/M_s indicate the fragmentation of martensite during its reversion. From the M_R/M_s behavior it has been noticed that drastic changes occur in the microstructure at 700 °C for very short times (~5 min). From

texture evaluation it was inferred that martensite reversion at 600 °C occurs by an athermal mechanism.

Acknowledgments

This work was partially supported by FAPESP – Sao Paulo Research Foundation (Brazil, Grant number 2013/26506-8). The authors thank to Dr. S. Romero for technical assistance and to Aperam South America (Brazil) for supplying the steel. IRSF thanks to CNPq – National Council for Scientific and Technological Development (Brazil, Grant 159.101/2013-1) and to Banco Santander S.A. (Brazil) for his scholarships. MJRS, HRZS, and LCCMN are CNPq Fellows. The Karlsruhe Institute of Technology is acknowledged for the use of its facilities.

References

[1] A.F. Padilha, R.L. Plaut, P.R. Rios, ISIJ Int. 43 (2003) 135.
[2] G. Zietek, Z. Mróz, Int. J. Struct. Change Sol. 3 (3) (2011) 21.
[3] L. Zhang, S. Takahashi, Y. Kamada, H. Kikuchi, K. Ara, M. Sato, T. Tsukada, J. Mater. Sci. 40 (2005) 2709.
[4] P.L. Mangonon Jr, G. Thomas, Metall. Trans. 1 (1970) 1577.
[5] M.W. Bowkett, S.R. Keown, D.R. Harries, Met. Sci. Technol. 16 (1982) 499.
[6] K. Mumtaz, S. Takahashi, J. Echigoya, Y. Kamada, L.F. Zhang, H. Kikuchi, K. Ara, M. Sato, J. Mater. Sci. 39 (2004) 85.
[7] J.Y. Choi, W. Jin, Scr. Mater. 36 (1) (1997) 99.
[8] E. Güller, T. Kirindi, H. Aktas, J. Alloy. Compd. 440 (2007) 168.
[9] S.S.M. Tavares, J.M. Neto, M.R. da Silva, I.F. Vasconcelos, H.F.G. Abreu, Mater. Charact. 59 (2008) 901.
[10] L.E. Murr, K.P. Staudhammer, S.S. Hecker, Metall. Trans. A 13A (1982) 627.
[11] L. Bracke, G. Mertens, J. Penning, B.C. Cooman, M. Liebeherr, N. Akdut, Metall. Mater. Trans. A – Phys. Metall. Mater. Sci. 37A (2006) 307.
[12] I. Mészáros, J. Prohászka, J. Mater. Process. Technol. 161 (2005) 162.
[13] S.S.M. Tavares, J.M. Pardal, M.J. Gomes da Silva, H.F.G. Abreu, M.R. da Silva MR, Mater. Charact. 60 (2009) 907.
[14] J.A. Lichtenfeld, M.C. Mataya, J.V. Tyne, Metall. Mater. Trans. A 37 (2006) 147.
[15] A. Kisko, R.D.K. Misra, J. Talonen, L.P. Karjalainen, Mater. Sci. Eng. A 578 (2013) 408.
[16] D. Maréchal, Linkage Between Mechanical Properties and Phase Transformation in a 301LN Austenitic Stainless Steel (Ph.D. thesis), The University of British Columbia, 2011.
[17] B.R. Kumar, A.K. Singh, B. Mahato, P.K. De, N.R. Bandyopadhyay, D. K. Bhattacharya, Mater. Sci. Eng. A 429 (2006) 205.
[18] A. Mitra, A. P. K. Srivastava, P.K. De, D.K. Bhattacharya, D.C. Jiles, Metall. Mater. Trans. A 35A (2004) 599.
[19] S.S.M. Tavares, M.R. da Silva, J.M. Neto, S. Miraglia, D. Fruchart, J. Magn. Magn. Mater. 242–245 (2002) 1391.
[20] B.D. Cullity, C.D. Graham, Introduction to Magnetic Materials, 2nd ed., John Wiley and Sons, New Jersey, 2009.
[21] J. Rys, W. Ratuszek, M. Witkowska, Arch. Metall. Mater. 51 (2006) 495.
[22] M. Elmassalami, I. Palatnik-de-Sousa, M.C.L. Areiza, J.M.A. Rebello, A. Elzubair, J. Magn. Magn. Mater. 323 (2011) 2403.
[23] C. Bormio-Nunes, O. Hubert, J. Magn. Magn. Mater. 393 (2015) 404.
[24] J. Charles, The new 200 series: an alternative answer to Ni surcharge? Dream or nightmare? in: Proceedings of the Fifth European Stainless Steel Science & Market Congress, Seville, September 27–30, 2005, pp. 19–28.
[25] S. Nanga, A. Pineau, B. Tanuy, P.O. Santacreu, Strain induced martensitic transformations in two austenitic stainless steels: macro-micro behavior, in: Proceedings of the 17th European Conference on Fracture, September 2–5, 2008, pp. 1373–1380.
[26] S. Papula, J. Talonen, H. Hänninen, Metall. Mater. Trans. A 45A (2014) 1238.
[27] A.S. Hamada, A.P. Kisko, P. Sahu, L.P. Karjalainen, Mater. Sci. Eng. A 628 (2015) 154.
[28] A.D. Schino, M.G. Mecozzi, M. Barteri, J.M. Kenny, J. Mater. Sci. 35 (2000) 375.
[29] P. Merinov, S. Entin, B. Beketov, A. Runov, NDT Int. 11 (1) (1978) 9.
[30] S. Baldo, I. Mészáros, J. Mater. Sci. 45 (2010) 5339.
[31] J. Talonen, H. Hänninen, Acta Mater. 55 (2007) 6108.
[32] A. Rezaee, A. Kermanpur, A. Najafizadeh, M. Moallemi, H. Samaei Baghbadorani, Mater. Des. 46 (2013) 49.
[33] B.R. Kumar, A.K. Singh, S. Das, D.K. Bhattacharya, Mater. Sci. Eng. A 364 (2004) 132.
[34] S.G. Chowdhury, S. Das, P.K. De, Acta Mater. 53 (2005) 3951.
[35] L. Xiao, Z. Fan, Z. Jinxiu, Z. Mingxing, K. Mokuang, G. Zhenqi, Phys. Rev. B 52 (1995) 9970.
[36] S.G. Chowdhury, S. Datta, B.R. Kumar, P.K. De, R.N. Ghosh, Mater. Sci. Eng. A 443 (2007) 114.
[37] M. Eskandari, M.A. Mohtadi-Bonab, R. Basu, M. Nezakat, A. Kermanpur, J. A. Szpunar, S. Nahar, A.H. Baghpanah, J. Mater. Eng. Perform. 24 (2014) 644.